Structural and magnetic properties of core–shell iron–iron oxide nanoparticles

L Theil Kuhn[1,4]**, A Bojesen**[1]**, L Timmermann**[1]**, M Meedom Nielsen**[2] **and S Mørup**[3]

[1] Ørsted Laboratory, Niels Bohr Institute for Astronomy, Physics and Geophysics, Universitetsparken 5, DK-2100 Copenhagen Ø, Denmark
[2] Danish Polymer Center, Risø National Laboratory, Frederiksborgvej 399, DK-4000 Roskilde, Denmark
[3] Department of Physics, Bldg 307, Technical University of Denmark, DK-2800 Kgs Lyngby, Denmark

E-mail: luise.theil.kuhn@risoe.dk

Abstract

We present studies of the structural and magnetic properties of core–shell iron–iron oxide nanoparticles. α-Fe nanoparticles were fabricated by sputtering and subsequently covered with a protective nanocrystalline oxide shell consisting of either maghaemite (γ-Fe_2O_3) or partially oxidized magnetite (Fe_3O_4). We observed that the nanoparticles were stable against further oxidation, and Mössbauer spectroscopy at high applied magnetic fields and low temperatures revealed a stable form of partly oxidized magnetite. The nanocrystalline structure of the oxide shell results in strong canting of the spin structure in the oxide shell, which thereby modifies the magnetic properties of the core–shell nanoparticles.

1. Introduction

Magnetic core–shell nanoparticles constitute systems with strong interactions between different magnetic and crystalline phases, which can result in exchange anisotropy and enhanced coercivity [1, 2]. From a technological point of view, the understanding of these magnetic properties is important. Often magnetic nanoparticles are covered with a protective shell when they are used in technological applications. For example, iron–iron oxide nanoparticles are used in magnetic recording tapes [2, 3]. Studies of oxidation of nanoparticles can also lead to improved understanding of corrosion processes.

As a consequence of their technological importance, iron–iron oxide nanoparticles have been investigated for decades. Several types of nanoparticle fabrication and structural and

---

[4] Present address: Materials Research Department, AFM-227, Risø National Laboratory, Frederiksborgvej 399, DK-4000 Roskilde, Denmark.

magnetic investigation techniques have been applied, see for instance [4–17]. There seems to be a general agreement that the iron core has the bulk structural and magnetic properties of α-Fe for a wide range of nanoparticle sizes and shapes, e.g. 2–30 nm spherical nanoparticles [4, 9, 11] and acicular nanoparticles 100–360 nm long with aspect ratios up to 20 [5, 6]. Furthermore, the iron oxide surface layer consists of nanocrystallites 2–5 nm in size [4–6], or for special oxide formation conditions an epitaxial layer of similar thickness [17]. Often a spinel type iron oxide has been observed, e.g. either maghaemite (γ-Fe$_2$O$_3$), magnetite (Fe$_3$O$_4$), non-stoichiometric partially oxidized magnetite or mixtures of them. The presence of wüstite (FeO) has also been reported [10].

The lattice constants of the spinel structures magnetite (Fe$_3$O$_4$) and maghaemite (γ-Fe$_2$O$_3$) are quite similar. Therefore, they are not easily distinguished by x-ray diffraction. Mössbauer spectroscopy is a well suited technique for distinguishing these two oxide phases. In maghaemite, the spectral components due to the Fe^{3+} ions in A- and B-sites have similar Mössbauer parameters and the spectrum can be described as a sextet, which is slightly asymmetric. Line 6 is slightly broader and less intense than line 1, because of the small differences between the isomer shifts and the magnetic hyperfine fields in the two sites. In magnetite, the B-sites contain equal amounts of Fe^{3+} and Fe^{2+} ions, but fast electron hopping between these ions results in an effective valence state, Fe$^{+2.5}$, for all B-site ions. The magnetic hyperfine field of B-site ions in magnetite is therefore smaller than that of the A-site ions (Fe^{3+}) and the isomer shift is larger. Thus, the A- and B-site contributions in the Mössbauer spectrum of magnetite can easily be distinguished. In bulk magnetite the electron hopping takes place only above the Verwey transition temperature, $T_V = 119$ K. Below this temperature, the Mössbauer spectrum consists of several sextets due to Fe^{2+} and Fe^{3+} ions. In nanoparticles of magnetite, the Verwey transition temperature is lower [18].

Mössbauer spectra with large applied magnetic fields give further information on the structure and magnetic properties of the iron oxides. Perfect magnetite and maghaemite have a collinear ferrimagnetic order. When the magnetization is saturated by a large applied field, the A-site hyperfine field will be parallel and the B-site hyperfine field anti-parallel to the applied field. Therefore, the magnetic splitting of the A component is increased and the splitting of the B component is decreased. This allows the A and B components in maghaemite to be distinguished if the applied field is sufficiently large. Furthermore, the relative intensities of lines 2 and 5 in the sextets will be affected by the applied field in a way that depends on the angle between the field direction and the direction of the gamma rays. If the sample is magnetized parallel to the gamma ray direction, lines 2 and 5 disappear in the spectrum. In small particles of magnetite and maghaemite, the spin structure is often non-collinear [19–23]. The canting may be localized at the nanoparticle surface, but defects in the interior of maghaemite nanoparticles may also induce canting [22, 23]. The spin canting can be studied by Mössbauer spectroscopy with large magnetic fields. The relative intensity of the six lines is given by 3:x:1:1:x:3 with

$$x = \frac{4\sin^2\theta}{1 + \cos^2\theta}, \tag{1}$$

where θ is the angle between the total magnetic field at the nucleus and the gamma ray direction [20]. Thus, the average canting angle can be estimated from the relative intensity of lines 2 and 5. Such studies are conveniently carried out with the applied field parallel to the gamma ray direction. The magnetic splitting is proportional to the total magnetic field at the nucleus, $\vec{B}_{tot}$, which is given by the vector sum of the hyperfine field, $\vec{B}_{hf}$, and the applied field, $\vec{B}_{app}$. Thus, B_{hf} can be found from the equation

$$B_{hf}^2 = B_{tot}^2 + B_{app}^2 - 2B_{tot}B_{app}\cos\theta. \tag{2}$$

We present here a combined structural and magnetic study of core–shell iron–iron oxide nanoparticles fabricated under different oxidation conditions. We have previously published results on the magnetic properties of single iron–iron oxide nanoparticles measured by Hall micro-magnetometry [25]. This study is focused on Mössbauer spectroscopy in the magnetic field range 0–6 T in the temperature range 5–295 K, and over a long time span (290 days). We contribute new results on the structural and the magnetic properties of the iron oxide surface layer.

The paper is organized as follows. In section 2 the experimental techniques are presented, in section 3 the crystal structure and the morphology of the nanoparticles is discussed and in sections 4 and 5 the magnetic properties are discussed. In section 6, the domain structure of the α-Fe core is investigated. In section 7 the stability of the core–shell nanoparticles is discussed. Section 8 concludes the paper.

2. Experimental techniques

2.1. Nanoparticles

The nanoparticles were fabricated in a hollow cathode sputtering cluster source, described in detail in [26]. A sputtering target (Fe) formed as a hollow cylinder was mounted in a condensation chamber and a sputtering gas (Ar, purity 99.998%) was led through at an applied high voltage. The sputtering process produced a supersaturated metal vapour, and by several stages of differential pumping of the Ar gas, the metal vapour was cooled and condensed into solid metal clusters. The system is designed such that the clusters form a beam with low kinetic energy and they can easily be deposited on any substrate without being damaged or damaging the substrate, nor do the nanoparticles agglomerate after deposition. The substrate was kept at room temperature. The cluster source vacuum system had a background pressure of 10^{-5} Pa, and during nanoparticle production the Ar pressure was in the range 60–500 Pa in the condensation chamber and in the differential pumping chambers it was reduced to 1, 10^{-2} and 10^{-4} Pa, respectively.

For the experiments presented here two different types of sample were fabricated. Sample A contained iron nanoparticles that were oxidized in a controlled way by exposing them to an increasing pressure of oxygen following the scheme in table 1 and subsequently exposed to air. Sample B was exposed to air immediately after fabrication. To produce Mössbauer absorbers with a homogeneous distribution of nanoparticles, the nanoparticles were mixed with a BN powder.

Table 1. Oxidation scheme for sample A. The total pressure of the oxygen–argon mixture was kept at 10^5 Pa.

O in Ar (mol%)	Time (h)
0.02	11.0
0.20	6.5
2.00	1.0

2.2. Structural characterization

The nanoparticles were structurally characterized by transmission electron microscopy (TEM) and x-ray powder diffraction. The TEM samples were prepared by deposition of the nanoparticles on thin substrates of amorphous carbon film. The TEM studies were done

with three instruments: a Philips CM20 (200 keV), a Philips EM430 (300 keV) and a Jeol 3000 F (300 keV). X-ray powder diffraction was done on specially prepared nanoparticle samples and on the as-prepared Mössbauer samples in a reflection geometry using a Rigaku Rotaflex 18 kW rotating anode with a Cu target. Pyrolithic graphite monochromators were used before and after the sample to select the Cu Kα radiation ($\lambda = 1.54(1)$ Å) and to suppress the Fe Kα fluorescence. The beam geometry was defined by slits. The instrument calibration and broadening was measured using a standard Si powder and the BN in the Mössbauer samples.

2.3. Mössbauer spectroscopy

Mössbauer spectra were obtained with a conventional constant-acceleration Mössbauer spectrometer using a 100 mCi source of ^{57}Co in Rh. Spectra below 20 K and all spectra with large applied fields (up to 6 T) were obtained using a liquid helium cryostat with a superconducting magnet. The magnetic field was applied parallel to the gamma ray direction. Zero-field spectra at $T \geqslant 20$ K were obtained in a closed-cycle helium refrigerator. Isomer shifts are given relative to that of α-Fe at room temperature. Room-temperature spectra with applied fields of 0.55 T perpendicular to the gamma ray direction were obtained by use of an electromagnet with an iron core.

3. Crystal structure and morphology of the nanoparticles

Figure 1 shows a TEM overview of sample A. The nanoparticles appear almost spherical, and those that have a crystal axis oriented along the electron beam direction show two contrasts, a dark iron core region and a light-grey oxide shell. The nanoparticles tend to form chains indicating a ferromagnetic interaction. The left-hand inset in figure 1 shows the electron diffraction pattern obtained from a large sample area with rings corresponding to the bulk bcc lattice structure of α-Fe with $a \simeq 2.9$ Å. Also a more diffuse diffraction ring pattern belonging to the oxide shell is visible. The right-hand inset in figure 1 shows the size distribution as determined by measuring the nanoparticle sizes on a series of TEM pictures. Fitting a lognormal distribution to the size distribution results in an average nanoparticle diameter of 21 nm and a logarithmic standard deviation $\sigma = 0.19$, where the iron core has an average diameter of 15 nm and the iron oxide shell has a thickness of 3 nm independent of the nanoparticle size.

Figure 2 shows a zoom by high-resolution electron microscopy on one of the larger nanoparticles (chosen here because of the better contrast). The iron core has eight facets suggesting a cuboctahedral shape, and dotted patterns originating from lattice planes in both the iron core and the iron oxide shell are visible. The lattice planes change direction in the oxide shell (compare A and B) indicating that it consists of several crystalline regions, i.e. nanocrystallites. In some regions (C) epitaxy between the iron core and the iron oxide shell appears to exist. Nanoparticles containing grain boundaries in the α-Fe cores were not observed.

TEM studies of sample B were only done directly on the Mössbauer sample. This complicated single-nanoparticle investigations, because of the dense mixture of nanoparticles and BN. It was, however, clear from the TEM pictures that the nanoparticles in sample B also consisted of an iron core and an iron oxide shell. The average diameter of the iron core and the thickness of the iron oxide shell was measured to be 28 and 5 nm, respectively, but the many overlapping nanoparticles increased the error in these measurements. Particularly the smaller nanoparticles and the oxide thickness were difficult to measure because of weak contrast in the TEM pictures.
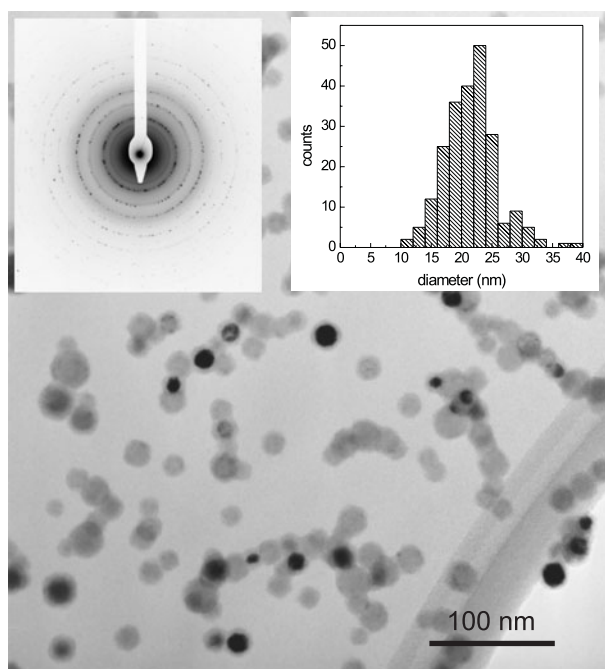
Figure 1. TEM picture of sample A; the left-hand inset shows the obtained electron diffraction pattern, and the right-hand inset shows the size distribution for sample A as determined from the TEM pictures.
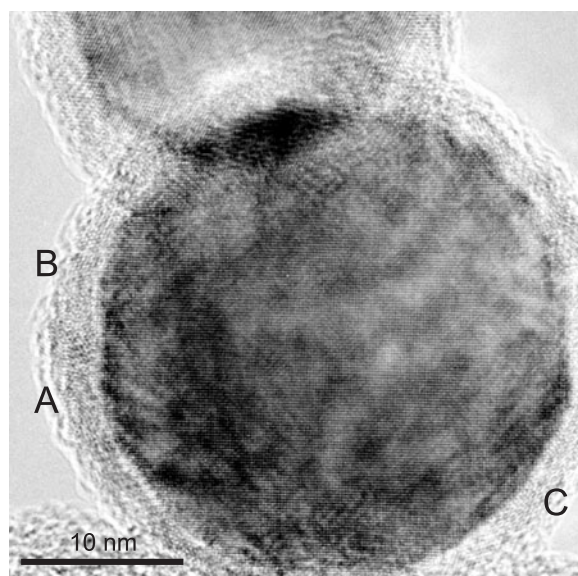
Figure 2. High-resolution electron microscopy picture of a single core–shell nanoparticle in sample A. The dark core is the α-Fe and the light shell is the γ-Fe$_2$O$_3$/Fe$_3$O$_4$. Lattice planes in both regions are visible. A smaller neighbouring nanoparticle is slightly overlapping at the top of the image. A–C refer to the text.
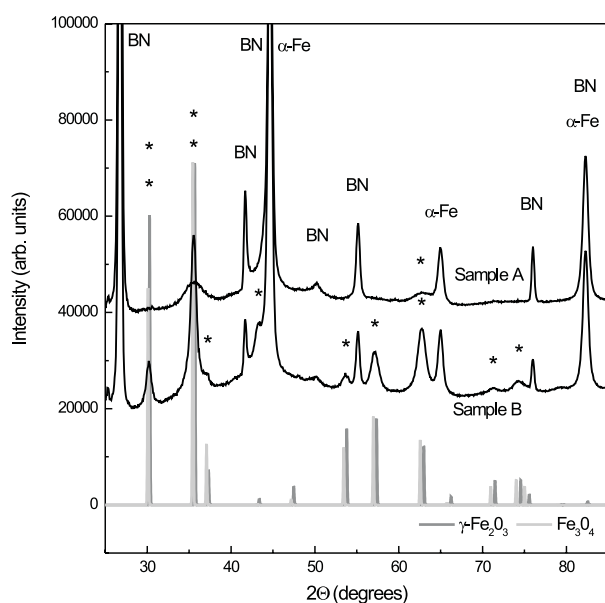
Figure 3. X-ray powder diffraction spectra from samples A and B. The background has been subtracted and the peaks are marked with their respective origins: BN, α-Fe and Fe_3O_4/γ-Fe_2O_3 with *. The spectra for A and B have been offset by 40 000 and 20 000, respectively. Also simulated spectra for bulk Fe_3O_4 and γ-Fe_2O_3 are plotted.

Figure 3 shows the x-ray powder diffraction spectra for samples A and B performed directly on the Mössbauer prepared samples; these also include BN. The background in the spectra has been measured and subtracted and the peaks are marked according to their origins: BN, α-Fe and Fe_3O_4/γ-Fe_2O_3 with *. Simulated spectra for the bulk spinel structures Fe_3O_4 ($a = 8.391$ Å) and γ-Fe_2O_3 ($a = 8.339$ Å) [27] are also shown. The small sizes of the nanoparticles introduce a significant size and strain broadening of the diffraction features, thereby making the two spinel iron oxides indistinguishable. The diffraction spectra show no traces of other iron oxides such as wüstite (FeO) or haematite (α-Fe_2O_3) nor other crystalline phases. The presence of the BN obstructed a valuable refinement of the spectra, therefore a more simplistic approach was chosen to evaluate the spectra: the background was subtracted and all the diffraction peaks were fitted with a sum of Gaussians and Lorentzians. The peaks originating from the nanoparticles were well fitted purely by Gaussians. The instrument broadening was subtracted from the nanoparticle peaks following $\Gamma_{cor} = \sqrt{\Gamma_{obs}^2 - \Gamma_{instr}^2}$, where Γ_{cor} is the corrected FWHM, Γ_{obs} is the observed FWHM and Γ_{instr} is the FWHM of the instrumental broadening. The average size of the crystalline regions was obtained using the Scherrer formula [28]

$$d = \frac{K\lambda}{\Gamma(2\theta)\cos(\theta)}, \tag{3}$$

where $K = 0.94$, $\lambda = 1.54$ Å and $\Gamma(2\theta)$ is the FWHM of the diffraction peaks at angle 2θ. The analysis showed that the Fe components in samples A and B are very similar and they originate from a bcc lattice with lattice constant $a = 2.87$ Å corresponding to bulk α-Fe [27]. For both samples, but particularly in sample B, an increasing broadening of the peaks with increasing 2θ beyond the instrumental broadening indicated the presence of

Table 2. Sizes as obtained with TEM and x-ray powder diffraction. Note that the numbers obtained by TEM for sample B are subject to a large error (see discussion in text).

	Sample A (nm)	Sample B (nm)
α-Fe d_{TEM}	15	28
α-Fe d_{x-ray}	18	18
Fe_3O_4/γ-Fe_2O_3 t_{TEM}	3	5
Fe_3O_4/γ-Fe_2O_3 t_{x-ray}	3	9

strain. However, an analysis of the strain based on the Williamson–Hall method [29] was not successful for the diffraction peaks, because of too large uncertainties on the fitting parameters. Therefore, the strain broadening has not been subtracted and the obtained nanoparticle diameters and oxide thicknesses represent lower limits. The average crystalline sizes for the α-Fe cores were obtained from three peaks for sample A (from the spectrum without BN, $2\theta = 44.7°$, $2\theta = 65.0°$ and $2\theta = 82.3°$), and for sample B from one peak ($2\theta = 65.0°$). The core sizes were $d \simeq 18$ nm for both samples, corresponding reasonably well with the TEM observations. We conclude that the iron core of the nanoparticles in both samples is single-crystalline α-Fe. The iron oxide components in the spectrum for sample B are much more intense and the peaks are narrower than for sample A. For sample A, fits were only possible for two peaks ($2\theta = 35.4°$ and $2\theta = 63.1°$); the obtained average iron oxide crystallite size was $t \simeq 3$ nm. This compares well to the oxide thickness obtained from the TEM pictures. For sample B six peaks ($2\theta = 30.2°$, $35.5°$, $53.7°$, $57.1°$, $62.8°$ and $74.4°$) could be fitted, and for this sample the average iron oxide crystallite size was $t \simeq 9$ nm. No evidence was found for preferred dimensions or orientations of the nanocrystallites. The sizes are summarized in table 2. The average nanoparticle size (core + shell) in sample B as determined with TEM was 38 nm, whereas x-ray powder diffraction gave a value of 36 nm. The weak contrast in the TEM pictures of overlapping nanoparticles only prevented a precise determination of the iron core size and the iron oxide shell thickness individually; the full average nanoparticle size seems reliable.

The x-ray powder diffraction was performed on as-prepared samples, after the Mössbauer spectroscopy measurements and again after 290 days after a second run of Mössbauer spectroscopy had been performed. No structural changes with time were observed.

4. Magnetic properties of the nanoparticles in sample A

Figure 4 shows Mössbauer spectra of sample A, obtained at 5 and at 150 K with and without an applied magnetic field of 6.0 T. The zero-field spectra show, besides the intense sextet due to α-Fe, another sextet with a larger hyperfine field, a larger isomer shift and broader lines, which is ascribed to the iron oxide surface layer. The Mössbauer parameters resulting from the fitting with Lorentzian lines are given in table 3. The parameters of the oxide component resemble well those of poorly crystalline maghaemite [23, 24, 30]. In the first attempts to fit the spectra, the relative areas of the lines of the sextets often had unrealistic values. Therefore, the area ratios were constrained to 3:x:1:1:x:3. In most fits the value of x was also constrained. These values are marked by an asterisk in table 3.

The hyperfine field in α-Fe is anti-parallel to the magnetization. Therefore, the application of a magnetic field of 6.0 T results in a reduction of the magnetic splitting of the α-Fe component by approximately 6 T. As will be discussed in section 6, the reduction in the hyperfine field may be slightly smaller than the applied field, because of the influence of the demagnetization field. Furthermore, fits of the α-Fe components show that the relative intensities of lines 2 and
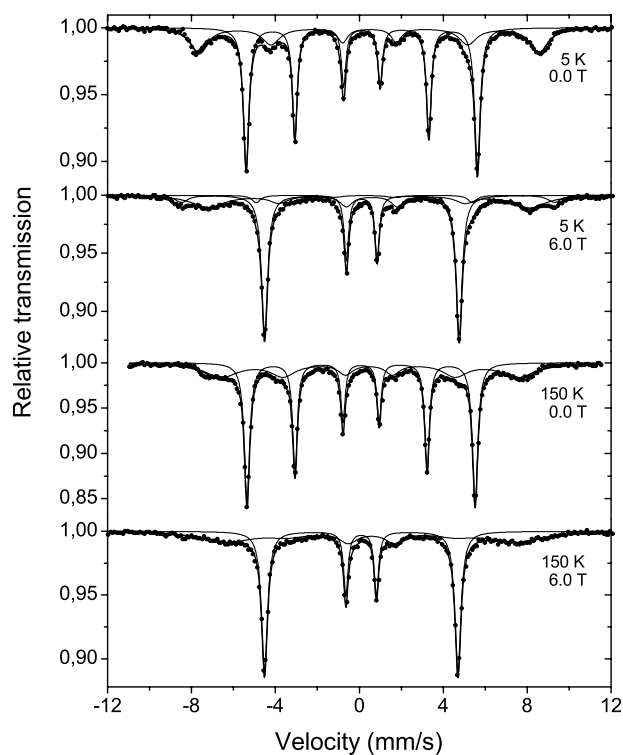
Figure 4. Mössbauer spectra for sample A for $T = 5$ and 150 K without magnetic field and in an applied field of 6.0 T. The dots represent the data and the lines represent the fitted sextets.

Table 3. Mössbauer parameters for sample A. T is the temperature, B_{app} is the applied magnetic field, B_{hf} is the hyperfine field, δ is the isomer shift, x is the area parameter in equation (1), A is the relative area and $\Gamma_{1,6}$ is the linewidth of lines 1 and 6. Numbers marked with an asterisk are constrained values (see the text).

T (K)	B_{app} (T)	B_{hf} (T)	δ (mm s^{-1})	x	A (%)	$\Gamma_{1,6}$ (mm s^{-1})
5	0.0	34.2	0.12	2.00*	64	0.32
		50.2	0.47	2.00*	36	1.00
5	6.0	28.8	0.12	0.00*	57	0.35
		55.1	0.32	2.00*	9	0.75
		47.6	0.52	0.96	34	1.90
150	0.0	33.7	0.08	2.00*	61	0.31
		43.9	0.48	2.00*	39	2.00
150	6.0	28.4	0.08	0.00*	56	0.34
		42.3	0.58	0.90	44	3.00

5 are negligible, showing that the α-Fe core is magnetically saturated. In the final fits, x was constrained to zero.

At 5 K, the applied field of 6.0 T results in a splitting of the oxide component into two sextets, one with an increased magnetic splitting and one with a reduced magnetic splitting. Because of the broad, overlapping lines in this component there is a considerable uncertainty in the fitting parameters for the oxide component. The appearance of two sextets in the oxide component does, however, show that the oxide component is ferrimagnetic. The hyperfine

fields are changed by less than the value of the applied field, and the non-zero relative intensity of lines 2 and 5 shows that there is a strong canting of the spins in the oxide. The relative area of the high-field component is apparently less than one-third of the relative area of the low-field oxide component in the 6.0 T spectrum. This is less than the expected values for perfect maghaemite ($\approx$0.6) or magnetite ($\approx$0.5). However, similar results were earlier found in studies of poorly crystalline maghaemite nanoparticles [23].

At 150 K, the lines of the oxide component in both the zero-field spectrum and the 6.0 T spectrum are considerably broadened, and it is not possible to distinguish two oxide sextets in the 6.0 T spectrum. The oxide component in this spectrum was therefore fitted with one sextet. The average hyperfine fields at 150 K are considerably smaller than those found at 5 K and also much smaller than the bulk value [31]. These observations can be explained by transverse relaxation, i.e. fluctuations of components of the magnetization, which are perpendicular to the direction of the average magnetization [30]. There is no indication of the presence of a sextet with hyperfine field and isomer shift corresponding to the $Fe^{2.5+}$ component in magnetite in the spectra obtained at 150 K. Thus the results indicate that the iron oxide shell covering the α-Fe nanoparticles in sample A consists of maghaemite with a disordered spin canted magnetic structure.

5. Magnetic properties of the nanoparticles in sample B

Mössbauer spectra of sample B, obtained without and with applied magnetic fields up to 6.0 T in the temperature range 5–295 K, are shown in figures 5 and 6, respectively. The fitting parameters of the Lorentzian lines for the corresponding spectra are given in table 4. The relative areas of the lines in the sextets were constrained as discussed in section 4.

As in the spectra for sample A an α-Fe sextet is present, but the spectra for sample B show a more pronounced pattern originating from the oxide. In the zero-field spectrum at 5 K, the oxide component can as a first approximation be described by one sextet. When a magnetic field of 6.0 T is applied, it splits up into two sextets in a way that is qualitatively similar to that seen for sample A. Both components exhibit spin canting, as evidenced from the non-zero values of the parameter x in table 4. At higher temperatures, the spectra of sample B are notably different from those of sample A. The zero-field spectra, obtained at $T \geqslant 100$ K, contain two oxide sextets with different isomer shifts and magnetic hyperfine fields. In fact, the Mössbauer parameters of the two sextets are similar to those of magnetite with the high-field component due to Fe^{3+} at the A-sites and the low-field component due to $Fe^{2.5+}$ at B-sites of the spinel lattice [24, 31]. In pure stoichiometric magnetite, the number of B-site iron atoms is twice the number of A-site iron atoms. The ratio of the spectral areas of the B and A components is therefore close to two. Although the uncertainty of the relative areas in the present case is large because of broad overlapping lines, the fits of the zero-field spectra indicate that the ratio is considerably smaller than 2. This shows that the iron oxide cannot be described as pure stoichiometric magnetite.

When large magnetic fields are applied at $T \geqslant 100$ K, the oxide component can be described as consisting of three sextets, in contrast to the spectrum of pure magnetite, which remains a superposition of two sextets. The analysis of the relative areas and the hyperfine parameters of these three components give new information on the composition of the oxide layer. For example, the spectra obtained at 150 K show for $B_{app} = 0$ T a component with a hyperfine field $B_{hf} = 46.7$ T and an isomer shift $\delta = 0.65$ mm s^{-1}, which are parameters very similar to those of the B-site $Fe^{2.5+}$ component of magnetite, but the lines are considerably broadened. When a magnetic field is applied, the magnetic splitting of this component is reduced, but the reduction is less than that corresponding to the value of the applied field.
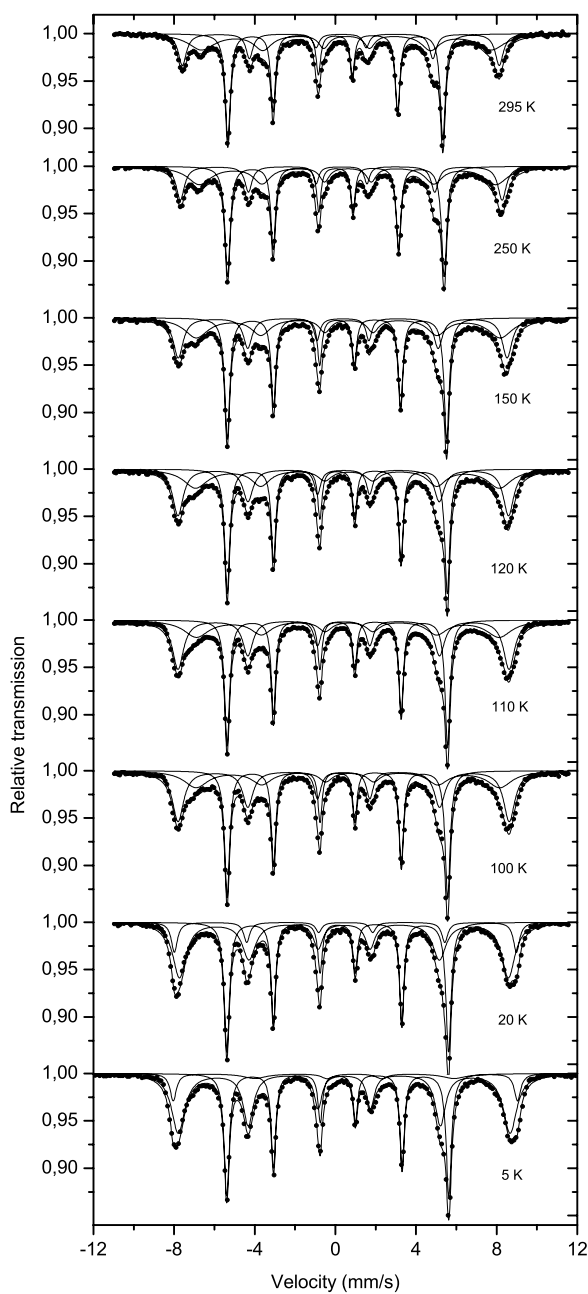
Figure 5. Zero field Mössbauer spectra for sample B in the temperature range 5–295 K. The dots represent the data and the curves represent the fitted sextets.

Furthermore, it is clear from the fits of the high-field spectra that there are significant intensities of lines 2 and 5. The relative intensities of these lines were constrained to 2.0 in order to avoid larger, physically unrealistic values. Both of these observations show, according to equations (1) and (2), that this component is strongly affected by spin canting. The relative intensity of this spin canted component is about 33% in all the spectra at 150 and 250 K.
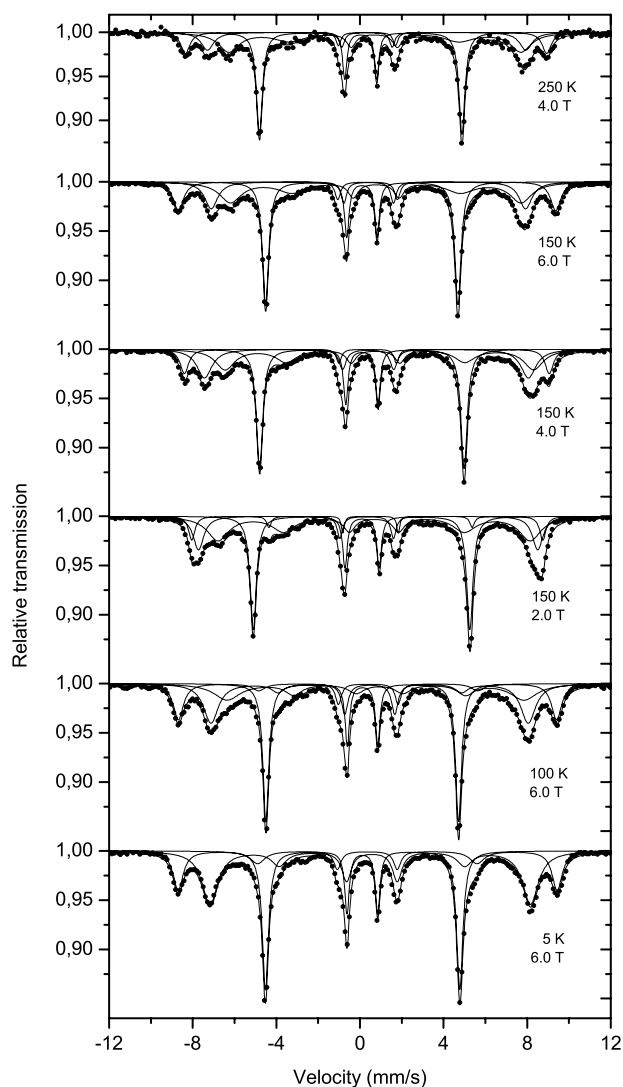
Figure 6. Mössbauer spectra for sample B showing the effect of applying a magnetic field up to 6.0 T at various temperatures between 5 and 250 K. The dots represent the data and the curves represent the fitted sextets.

The second iron oxide component, seen in the zero-field spectrum at 150 K, has a magnetic hyperfine field $B_{hf} = 50.6$ T and an isomer shift $\delta = 0.37$ mm s^{-1}. These values are close to those for Fe^{3+} in A-sites in magnetite and for Fe^{3+} ions in both A-sites and B-sites in maghaemite. When magnetic fields are applied, the component splits up into two sextets. At $B_{app} = 6.0$ T, the magnetic splittings of the two components are increased or decreased by amounts corresponding to approximately the value of the applied field. The spectra are well fitted with zero intensity of lines 2 and 5 in these two components. These results show that the Fe^{3+} ions are distributed between A- and B-sites. The relative areas of the two Fe^{3+} sextets are similar, indicating that the numbers of Fe^{3+} ions on A-sites and B-sites are similar. The spectra obtained at 100 K show the same trends, but as the linewidths are larger at this temperature, the

Table 4. Mössbauer parameters for sample B. T is the temperature, B_{app} is the applied magnetic field, B_{hf} is the hyperfine field, δ is the isomer shift, x is the area parameter in equation (1), A is the relative area and $\Gamma_{1,6}$ is the linewidth of lines 1 and 6. Numbers marked with an asterisk are constrained values (see the text).

T (K)	B_{app} (T)	B_{hf} (T)	δ (mm s^{-1})	x	A (%)	$\Gamma_{1,6}$ (mm s^{-1})
5	0.0	34.1	0.12	2.00*	40	0.31
		51.0	0.44	2.00*	49	0.80
		53.0	0.72	2.00*	11	0.37
5	6.0	28.8	0.12	0.00*	36	0.36
		47.5	0.53	0.74	42	0.92
		56.2	0.36	1.36	22	0.58
100	0.0	33.9	0.10	2.00*	40	0.30
		46.6	0.67	2.00*	24	1.42
		50.9	0.41	2.00*	36	0.67
100	6.0	28.6	0.11	0.00*	33	0.35
		44.0	0.84	1.24	23	1.53
		47.1	0.46	0.54	27	0.85
		56.1	0.38	0.72	17	0.59
150	0.0	33.7	0.08	2.00*	41	0.30
		46.7	0.65	2.00*	32	1.45
		50.6	0.37	2.00*	27	0.59
150	2.0	32.1	0.09	0.00*	35	0.36
		46.3	0.67	2.00*	38	1.24
		50.3	0.35	0.00*	18	0.61
		52.1	0.42	1.02	9	0.36
150	4.0	30.3	0.09	0.00*	38	0.36
		45.8	0.83	2.00*	30	1.12
		48.1	0.35	0.00*	10	0.48
		54.1	0.35	0.00*	10	0.48
150	6.0	28.5	0.09	0.00*	37	0.35
		43.1	0.77	2.00*	32	1.26
		46.6	0.41	0.00*	17	0.74
		56.0	0.35	0.00*	14	0.60
250	0.0	33.3	0.02	2.00*	45	0.31
		45.6	0.61	2.00*	33	1.43
		49.5	0.30	2.00*	22	0.48
250	4.0	30.0	0.04	0.00*	38	0.34
		43.3	0.70	2.00*	36	1.18
		47.2	0.33	0.00*	14	0.72
		53.6	0.31	0.00*	12	0.52

uncertainties are larger. The results obtained at 250 K are also consistent with those obtained at 150 K.

The data obtained above 100 K may be explained by the presence of a mixture of maghaemite and magnetite or by a partially oxidized magnetite. It is difficult to distinguish between these from high-field Mössbauer spectra above the Verwey temperature [32]. However, the spectra obtained at lower temperatures can further elucidate the nature of the oxide shell.

It is surprising that although there is a substantial number of $Fe^{2.5+}$ ions visible in the spectra obtained at $T \geqslant 100$ K, there are no visible Fe^{2+} lines in the spectra obtained at 5 K. In perfect bulk magnetite, the Verwey transition is a first-order transition, which takes place at $T = 119$ K. In nanoparticles, the transition takes place at a lower temperature than in

bulk. Earlier studies of magnetite nanoparticles as small as 6 nm have shown the presence of a Verwey transition such that the 5 K spectrum of the nanoparticles was almost identical to that of bulk magnetite with several visible lines due to Fe^{2+} [18]. The magnetic hyperfine fields of the Fe^{2+} components, which were expected to be visible at 5 K, are very sensitive to local distortions caused by, for example, defects, because of the orbital contribution to the magnetic hyperfine field. Therefore, if there are variations of the local environments of the Fe^{2+} ions, the Fe^{2+} components may be smeared out such that they are not visible as separate components. The results of the present study therefore indicate that the oxide component is not a mixture of magnetite and maghaemite, but rather a partly oxidized magnetite.

6. Demagnetization fields in the α-Fe cores

Small ferromagnetic particles may be single-domain or multi-domain particles depending on the particle size. In single-domain particles, the atoms in the interior are exposed to the demagnetizing field, which is formed by the uncompensated poles at the surface. The value depends on the nanoparticle shape, the magnetization and the magnetization direction. The demagnetizing field is anti-parallel to the magnetization direction. For spherical single-domain α-Fe nanoparticles, the demagnetizing field equals 0.7 T [33, 34]. For an infinite film magnetized in the film plane, the demagnetizing field vanishes. If a nanoparticle is large enough to form domains, the poles at the surface may disappear, resulting in the disappearance of the demagnetizing field. If a multi-domain particle is exposed to a sufficiently large magnetic field, the domain structure is broken down such that it becomes a single-domain particle with a non-zero demagnetization field [33].

In ^{57}Fe Mössbauer spectroscopy one can measure the magnetic field at the nuclei with a precision better than 0.05 T. Therefore, Mössbauer spectroscopy of ferromagnetic materials can be used to study demagnetizing fields, i.e. it can give information on the domain structure of small particles [33, 34]. If the ferromagnetic nanoparticles are not well separated, the nuclei will also feel a magnetic field arising from the dipole field of the neighbouring nanoparticles. The total contribution to the field at a nucleus in a spherical nanoparticle is given by [33, 34]

$$\vec{B}_{tot} = \vec{B}_{hf} + \vec{B}_{dem} + \vec{B}_{dip} + \vec{B}_{app}. \tag{4}$$

The first term represents the hyperfine field, the second term the demagnetizing field, the third term the dipole field from the neighbouring nanoparticles and the fourth term the applied field. Calculating the dipole term is complicated since it depends on the geometrical arrangement and the orientation of the magnetization of the neighbouring nanoparticles.

To get information about the domain structure of the α-Fe cores in our samples, we have obtained room-temperature Mössbauer spectra with and without a magnetic field of 0.55 ± 0.01 T applied parallel to the sample plane. Similar measurements were made on a thin calibration foil of α-Fe. The values of B_{tot} for the α-Fe components are given in table 5. The uncertainty on B_{tot} is 0.03 T. For the iron foil, the application of the magnetic field results in a reduction of B_{tot} by 0.54 T, which is very close to the value of the applied field. This is as expected because the demagnetizing field is close to zero for a thin foil. For samples A and B, B_{tot} is *reduced* by only 0.17 and 0.16 T, respectively, when the magnetic field is applied.

Based on the structural characterization we can assume that the nanoparticles are close to being spherical. The contributions of the applied field and the demagnetizing field should therefore result in an *increase* of B_{tot} by 0.15 T. These results suggest that the dipole field from neighbouring nanoparticles is *not negligible*, and it is approximately 0.3 T. Earlier experimental studies as well as Monte Carlo simulations on samples of non-oxidized α-Fe nanoparticles arranged in chains yielded values of about 0.4 T for the dipole interaction [34]. The lower value
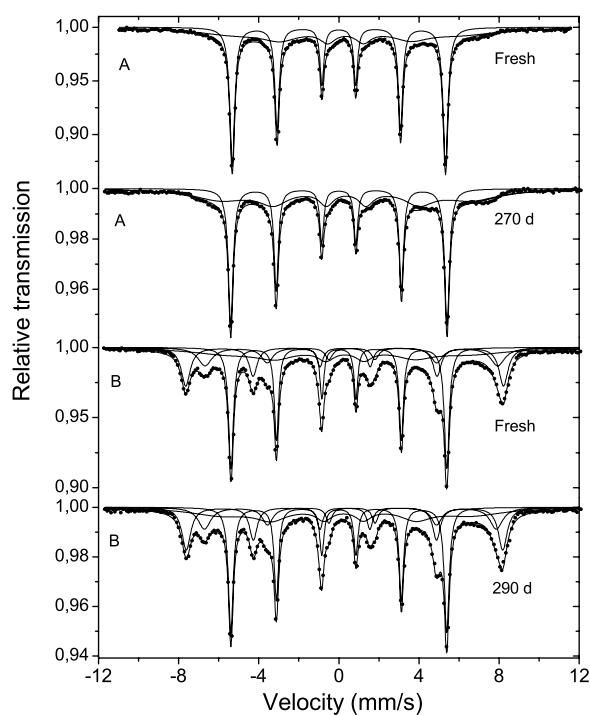
Figure 7. Mössbauer spectra for sample A (upper) and sample B (lower) at room temperature without magnetic field applied. The spectra were recorded when the samples were fresh and after 270 and 290 days, respectively. Sample B particularly shows perfect stability in time. The dots represent the data and the curves represent the fitted sextets.

Table 5. The total measured magnetic field B_{tot} at the Fe nucleus for a calibration foil of α-Fe and for samples A and B obtained at room temperature with and without an applied magnetic field.

Sample	B_{app} (T)	B_{tot} (T)
Cal. foil	0.00	33.14
Cal. foil	0.55	32.60
Sample A	0.00	33.25
Sample A	0.55	33.08
Sample B	0.00	33.22
Sample B	0.55	33.06

in the present study can in part be explained by the different geometrical arrangement in our powder samples and in part by the presence of oxide surface layers, which reduce the magnetic interactions. It should be noticed that for zero applied field, the values of B_{tot} for samples A and B are slightly larger than that of the iron foil. It is very likely that the nanoparticles form an imperfect single-domain structure due to their size, e.g. a vortex-like spin structure as suggested by previous magnetization measurements on similar nanoparticles [25]. This may influence the demagnetizing field at zero applied magnetic field.

7. Stability of the oxide shell

From the Mössbauer fitting parameters of the 5 K spectra given in tables 3 and 4 we observe that the area fractions for the iron and the iron oxide components are $A_{iron,A} = 64(5)\%$

and $A_{oxide,A} = 36(5)\%$, and $A_{iron,B} = 40(5)\%$ and $A_{oxide,B} = 60(5)\%$ for samples A and B, respectively[5]. Thus, we can estimate the thickness of the iron oxide shell assuming that the sizes of iron cores obtained by x-ray powder diffraction are correct, and that the bulk densities apply to our nanoparticles ($\rho_{iron} = 7848$ kg m^{-3}, $\rho_{maghaemite} = 5490$ kg m^{-3} and $\rho_{magnetite} = 5210$ kg m^{-3} [27]). Then, for sample A the thickness of the maghaemite shell becomes $t_A \simeq 3$ nm, and for sample B the partly oxidized magnetite shell thickness becomes $t_B \simeq 6$ nm. Taking the uncertainties into account, this agrees well with the results of the structural characterization by TEM and x-ray powder diffraction.

It is important to note that within the experimental error, the total areas in the Mössbauer spectra do not show any substantial temperature dependence in the measured temperature range 5–295 K, and the Debye–Waller factor is not much different from that of the bulk material. Furthermore, the area fractions for both samples A and B show no change in the temperature range 5–295 K. This means that the effective Debye–Waller factors, and thereby also the effective Debye temperatures, for the iron core and the iron oxide shell are equal. This is in opposition to the results of some earlier studies [7, 8], where it was observed that the iron oxide nanocrystallites had a lower apparent Debye temperature than the α-Fe core, i.e. the iron oxide nanocrystallites were slightly detached from the iron core and could vibrate separately.

Immediately after the samples were prepared, they were transferred to vacuum, and the measurements at both room temperature and lower temperature were carried out in vacuum in order to limit further oxidation during the measurements. After most of the low-temperature measurements had been carried out, the samples were kept in air and occasionally a Mössbauer spectrum was recorded at room temperature in order to follow the oxidation of the nanoparticles. Figure 7 shows room-temperature Mössbauer spectra of samples A and B as freshly prepared and after 270 and 290 days, respectively. In sample A, there seems to be a small increase in the amount of oxide. The lines of the oxide component appear to become sharper and more intense after the long exposure to air as also observed in [11]. However, the fits of the spectra did not give clear evidence for a change of the area ratio of the α-Fe component and the oxide component. Sample B seems very little affected by the exposure to air. This means that the relative amount of oxidized iron is close to being constant. Furthermore, the degree of oxidation of the partially oxidized magnetite is also found to be unaffected by the exposure to air.

The evolution with time t of the oxidation of Fe can be described by the Carberra–Mott equation [11]

$$t = \frac{x^2}{Ax_0}e^{-x_0/x}, \tag{5}$$

where x is the thickness of the formed oxide layer, $x_0 = 8 \times 10^{-8}$ m is a material constant for the oxide and $A \simeq 5.4 \times 10^{-30}$ m s^{-1} is the growth velocity constant. These constants are valid at $T = 295$ K. This means that the α-Fe nanoparticle oxide evolves from 1 nm at $t = 0.2$ fs to 2 nm at $t = 40$ s and to 3 nm at $t = 40$ weeks. At higher temperature the oxide grows faster.

Comparing the structural and magnetic properties of samples A and B, the observation of the thick, extremely stable, partly oxidized magnetite shell is striking. We suggest that the nanoparticles in sample A behave and evolve as expected according to the Carberra–Mott model because the oxide shell was formed under controlled conditions, whereas the sudden exposure to air for sample B caused the nanoparticles to oxidize in a very abrupt way presumably under elevated temperature for a short while (other samples were observed to burst into sparks when

---

[5] The error on the area fractions for the fitted iron sextets is approximately ±5%. On the individual oxide components the error is in some cases larger because of the very broad lines.

suddenly exposed to air). As the nanoparticles were cooled by the surrounding air, the violent oxidation stopped and an iron oxide in a frozen state resulted.

8. Conclusion

In conclusion, we have observed that facetted single-crystalline α-Fe nanoparticles exposed to different oxidation conditions formed different phases of nanocrystalline iron oxide shells. The core–shell nanoparticles proved to be structurally strained and very rigid, and we suggest that this is caused by the perfect crystallinity and purity of the iron nanoparticles before the oxide was formed. The iron oxide shell formed under controlled oxidation conditions in an oxygen/argon atmosphere at room temperature was shown to be maghaemite (γ-Fe$_2$O$_3$). The maghaemite shell grew very slowly in time. The iron oxide shell formed when the iron nanoparticles were exposed to sudden violent oxidation in air consisted of a partly oxidized phase of magnetite (non-stoichiometric Fe$_3$O$_4$), which proved to be extremely stable in time. This particular frozen form of partly oxidized magnetite was revealed through Mössbauer spectroscopy between 5 and 295 K in applied magnetic fields up to 6 T.

The Mössbauer spectra showed that the nanoparticles in both samples A and B behaved like ferromagnetic cores with strongly frustrated spin canted magnetic shells, and no superparamagnetic effects were observed. This all points to the presence of strong magnetic interactions between the α-Fe core and the γ-Fe$_2$O$_3$ and the Fe$_3$O$_4$ shells. The analysis of the demagnetization measurements indicated that the iron core of the nanoparticles formed an imperfect single-domain structure, and that the iron oxide surface layer reduced the magnetic interactions between the nanoparticles.

Acknowledgments

References

[1] Cullity B D 1972 *Introduction to Magnetic Materials* (Reading, MA: Addison-Wesley)
[2] O'Handley R 2000 *Modern Magnetic Materials* (New York: Wiley)
[3] Morales M P, Walton S A, Prichard L S, Serna C J, Dickson D P E and O'Grady K 1998 *J. Magn. Magn. Mater.* **190** 357
[4] Haneda K and Morrish A H 1978 *Surf. Sci.* **77** 584
[5] Kishimoto M, Kitahata S and Amemiya M 1986 *IEEE Trans. Magn.* **200** 732
[6] Maeda Y, Aramaki M, Takashima Y, Oogai M and Goto T 1987 *Bull. Chem. Soc. Japan* **60** 3241
[7] Tamura I and Hayashi M 1992 *Japan. J. Appl. Phys.* **31** 2540
[8] Huang R, Xiong H, Lu Q, Hsia Y, Liu R, Ji R, Lu H, Wang L, Xu Y and Fang G 1993 *J. Appl. Phys.* **74** 4102
[9] Bødker F, Mørup S and Linderoth S 1994 *Phys. Rev. Lett.* **72** 282
[10] Sethi S A, Pedersen M S, Thölen A R and Mørup S 1994 *Nanophase Materials* ed G C Hadjipanayis and R W Siegel (Dordrecht: Kluwer) p 81
[11] Linderoth S, Mørup S and Bentzon M D 1995 *J. Mater. Sci.* **30** 3142
[12] Parker F T, Spada F E, Cox T J and Berkowitz A E 1995 *J. Appl. Phys.* **77** 5853
[13] Jönsson B J, Turkki T, Ström V, El-Shall M S and Rao K V 1996 *J. Appl. Phys.* **79** 5063
[14] Zhao X Q, Liu B X, Liang Y and Hu Z Q 1996 *J. Magn. Magn. Mater.* **164** 401
[15] Kim H-J, Park J-H and Vescovo E 2000 *Phys. Rev.* B **61** 15284
[16] Banarjee S, Roy S, Chan J W and Chakravorty D 2000 *J. Magn. Magn. Mater.* **219** 45

[17] Kwok Y S, Zhang X X, Qin B and Fung K K 2000 *Appl. Phys. Lett.* **77** 3971
[18] Mørup S and Topsøe H 1983 *J. Magn. Magn. Mater.* **31–34** 953
[19] Coey J M D 1971 *Phys. Rev. Lett.* **27** 1140
[20] Morrish A H and Haneda K 1983 *J. Magn. Magn. Mater.* **35** 105
[21] Coey J M D 1987 *Can. J. Phys.* **65** 1210
[22] Morales M P, Serna F, Bødker F and Mørup S 1997 *J. Phys.: Condens. Matter* **9** 5461
[23] Serna C J, Bødker F, Mørup S, Morales M P, Santiumenge F and Veintemillas-Verdaguer S 2001 *Solid State Commun.* **118** 437
[24] de Grave E, da Costa G M, Bowen L H, Barrero C A and Vandenberghe R E 1998 *Hyperfine Interact.* **117** 245
[25] Kuhn L T, Geim A K, Lok J G S, Hedegård P, Ylänen K, Jensen J B, Johnson E and Lindelof P E 2000 *Eur. Phys. J.* D **10** 259
[26] Kuhn L T 1999 *PhD Thesis* University of Copenhagen
[27] Mineral database on www.webmineral.com
[28] Warren B E 1990 *X-Ray Diffraction* (New York: Dover)
[29] Gerward L 2001 *X-Ray Analytical Methods* (Kgs. Lyngby: Technical University of Denmark)
[30] Tronc E, Ezzir A, Cherkaoui R, Chanéac C, Noguès M, Kachkachi H, Fiorani D, Testa A M, Grenèche J M and Jolivet J P 2000 *J. Magn. Magn. Mater.* **221** 63
[31] Murad E 1998 *Hyperfine Interact.* **111** 251
[32] Vandenberghe R E, Barrero C A, da Costa G M, Van San E and de Grave E 2000 *Hyperfine Interact.* **126** 247
[33] Knudsen J E and Mørup S 1980 *J. Physique* **41** C1-155
[34] von Eynatten G and Bömmel H E 1977 *Appl. Phys.* **14** 415